Computers & Industrial Engineering 200 (2025) 110753



Contents lists available at ScienceDirect

Computers & Industrial Engineering

journal homepage: www.elsevier.com/locate/caie





EWMA control chart framework for efficient Maxwell quality characteristic monitoring: An application to the aerospace industry

Zahid Khan [a], Aamir Saghir [b], Attila Katona [a], Zsolt T. Kosztyán [a,*]

[a] Department of Quantitative Methods, University of Pannonia, Egyetem str. 10., Veszprém, Hungary
[b] Department of Statistics Mirpur University of Sciences and Technology, Mirpur, Pakistan

ARTICLE INFO

Keywords:
Maxwell quality characteristic
Skewed data
Estimation
Control chart
Run length
Simulation

ABSTRACT

The Maxwell distribution is extensively employed in statistical modeling to analyze data, notably in the fields of chemistry, astrophysics, demography, actuarial sciences, economics, industry, and engineering. Recently, the application of the Maxwell data generating process (DGP) has focused extensively on the domain of statistical control charts. The V chart and V_{SQ} chart are often used to identify unexpected changes in the distributional shift of the Maxwell process. The V_{SQ} chart offers considerably better performance than the V chart for detecting moderate to large shifts in the scale parameter. However, the V_{SQ} chart adopts the fundamental structure of the Shewhart monitoring scheme and is insensitive to small alterations in the target parameter. We propose a new control chart, namely, the Maxwell exponentially weighted moving average (MXEWMA) chart, for improved monitoring of quality attributes that are assumed to conform to Maxwell data generation. The factors used to design the parameters of the proposed chart are computed at different false alarm probabilities and across various sample sizes. The effectiveness of the suggested scheme is considered in terms of the different features of the run length (RL) distribution, including the average, median and standard deviation. A comparative study of the MXEWMA chart with the existing V_{SQ} chart was performed across various sample sizes. The comparative analysis showed that the MXEWMA chart is an effective alternative and performs well in detecting reasonably small shifts in the parameter. Simulated data are employed to describe the computational procedure of the MXEWMA scheme. The simulation analysis demonstrated that the MXEWMA chart outperforms the existing method in identifying slight changes in the studied parameters. A real dataset is also considered to support the theoretical part of the work.

1. Introduction

The control chart approach is used to monitor sequential processes such as internet traffic, production lines, power supply, economic or social status, and medical systems to ensure that they run satisfactorily and stably (Bogo et al., 2023). It is a central component of statistical process control (SPC) and is utilized by quality control management to maintain the quality parameters of the underlying processes (Ahmed et al., 2024). The quality of a manufacturing process is assessed by the quality of the items produced (Mahmood & Erem, 2023). A high-quality manufacturing process can result in high-quality items overall (Abbas, Abbas et al., 2024). Control charts may be used to eliminate certain frequent causes of variation, which would enhance the quality of the manufacturing process (Abbas, 2018). The Shewhart charting scheme, initially developed by Montgomery (2019), is widely used for process monitoring because it is simple to use and easy to implement (Mehmood et al., 2023; Riaz & Does, 2009). Additionally, and perhaps more crucially, Shewhart-type charts are sensitive to significant changes in process parameters (Javed et al., 2024). Despite their widespread popularity and simplicity, Shewhart charts are rarely employed in industrial processes and service businesses because even minor process changes might result in significant financial penalties (Ahmed et al., 2020; Katona et al., 2023; Kosztyán & Katona, 2018). Therefore, the use of memory-type control charts (e.g., EWMA charts and CUSUM charts), which are more responsive to small-to-moderate changes in the monitored parameters (Alevizakos et al., 2022). These kinds of charts use both new and old data to keep an eye on objects in real time, which makes them more aware of and able to react to small changes in the process parameters.

Control charts are frequently utilized in supervisory processes under the assumption that the observed quality characteristics adhere to normality (Nazir et al., 2021). Numerous real-world quality characteristics

* Corresponding author.
E-mail addresses: zainkhan@hu.edu.pk (Z. Khan), aamirstat@yahoo.com (A. Saghir), katona.attila@gtk.uni-pannon.hu (A. Katona), kosztyan.zsolt@gtk.uni-pannon.hu (Z.T. Kosztyán).

https://doi.org/10.1016/j.cie.2024.110753
Received 13 May 2024; Received in revised form 18 September 2024; Accepted 20 November 2024
Available online 2 December 2024
0360-8352/© 2024 The Authors. Published by Elsevier Ltd. This is an open access article under the CC BY license (http://creativecommons.org/licenses/by/4.0/).

follow asymmetric distributions. In such circumstances, process charts constructed under the supposition of normality may result in misleading judgments about the state of a process (Abbas et al., 2019; Abbasi & Miller, 2012). In recent years, some works on EWMA design have focused widely on underlying processes that follow certain nonnormal DGPs. In this context, numerous studies have been carried out on the basic structure of the EWMA chart and its enhanced variants to track nonnormal processes. Notably, works by Alduais and Khan (2023), Nawaz et al. (2021), Noiplab and Mayureesawan (2019) and Teoh et al. (2023) have contributed significantly to this area. Additionally, The robustness of EWMA control charts when considering heavy-tailed and skewed distributions was investigated by Human et al. (2011). Liu et al. (2007) studied the Weibull distribution and the transformed exponential distribution for robust EWMAs. Ryan and Woodall devised another robust design for Poisson processes (Ryan & Woodall, 2010). The construction of an EWMA for binomial observations was presented by Gan (1990). In the case of numerous other nonnormal distributions, Adeoti (2020) and Maravelakis et al. (2005) investigated the applicability of EWMA charts. Raza et al. (2016) developed an EWMA chart via a multivariate version of the gamma distribution and Student's t distribution. For several other applications of enhanced EWMA design for underlying nonnormal processes, readers are referred to Abbas et al. (2023, 2011), Haq et al. (2019), Nazir et al. (2021), Saghir, Ahmad et al. (2021) and Sanaullah et al. (2024). There remains a significant gap in the literature regarding studies on control charts specifically designed for nonnormal data-generating models.

By prioritizing nonnormality assumptions in control chart development, several researchers have proposed control charts for Maxwell family processes. For example, Godase et al. (2022) proposed one-sided and two-sided SPRT control charts for monitoring the scale parameter of a Maxwell distributed process. Additionally, Hossain et al. (2019) designed a VCUSUM chart, a variant of the CUSUM chart, specifically for monitoring the scale parameter of the Maxwell distribution. Saghir, Abbasi et al. (2021) studied the V control chart in situations where the parameter is estimated. Furthermore, Kapase and Ghute (2024) investigated methods for estimating the exact time of a process shift to enable quick identification of root causes in the Maxwell DGP. Arafat et al. (2019) introduced the IMEWMA chart to specifically monitor the scale parameter when the quality characteristic follows the inverse Maxwell distribution. Another extended AIMEWMA scheme for inverse Maxwell quality characteristics was devised by Saghir et al. (2023). The quality characteristic exhibits an inverse Maxwell distribution, known for its heavier tails than the Maxwell distribution. Extensive theoretical properties of the inverse Maxwell distribution have been discussed in the literature, with studies focusing on its distributional properties, extended versions, and parameter estimation techniques (Al-Kzzaz & Abd El-Monsef, 2022; Sharma et al., 2018). However, real-life applications of this distribution in statistical applications are considerably limited compared with the more commonly used Maxwell distribution (Tomer & Panwar, 2020). The Maxwell distribution is a widely used statistical model, particularly in the fields of chemistry, statistical mechanics, and reliability analysis. Referring to Maxwell processes, the V-chart was developed by Hossain et al. (2017) to monitor the parameters of the underlying Maxwell process. The methodology of the V-chart is rooted in the monitoring scheme of the basic Shewhart model. A memory type control of the V chart known as the VEWMA chart was proposed by Hossain and Riaz (2021). In practical scenarios, there is sometimes a preference to directly evaluate the scale parameter of Maxwell distributed data instead of its squared counterpart. This approach forms the basis of the V_{SQ} chart, which involves directly monitoring the Maxwell scale parameter (Shah et al., 2021). The V_{SQ} chart is an enhanced alternative proposed for identifying minute shifts in the target parameter of a Maxwell process. The studies mentioned earlier motivated our interest in exploring the application of the EWMA framework in the V_{SQ} chart. The V_{SQ} chart uses the standard Shewhart model, which is more suitable for detecting larger process shifts. However, there is a notable gap in the literature regarding control chart design for identifying smaller process changes within the same framework. Compared with the Shewhart model, the EWMA structure is recognized for its superior ability to detect minor shifts in process parameters. To our knowledge, no EWMA-based V_{SQ} chart has been developed for the Maxwell scale parameter.

This study addresses a gap in the literature by introducing the Maxwell exponential weighted moving average (MXEWMA) chart. The proposed MXEWMA efficiently monitors the scale parameters of Maxwell processes, particularly for detecting minor shifts. This fills a critical need for effective monitoring of the Maxwell DGP, enhancing the performance across various shift magnitudes. The main contributions of this work are as follows:

(1) A novel and efficient design is proposed for monitoring subtle process changes in systems that follow the Maxwell distribution.
(2) The design parameters and performance indicators of the suggested MXEWMA chart are thoroughly examined through Monte Carlo simulations.
(3) The practical usefulness of the MXEWMA chart is provided via real-world industrial data.

The framework of this paper is as follows: Preliminary results are presented in Section 2. The proposed MXEWMA model is established in Section 3. The assessment and evaluation of the MXEWMA model are covered in Section 4. Simulation analysis is conducted in Section 5. In Section 6, the proposed design is compared and contrasted with other approaches. The impact of estimation on the performance of the control chart is examined in Section 7. The model's actual data application for industrial problems is demonstrated in Section 8. Section 9 provides a final summary.

2. Preliminaries

In this section, we provide a brief explanation of the Maxwell distribution and present it within a comprehensive framework. The subsequent concepts establish a connection between understanding the underlying process of generating Maxwell data and practical applications in SPC.

The distribution function (DF) and probability density function (PDF) with a single scale parameter of the Maxwell model are denoted by the following expressions (see Eqs. (1)–(2)):

$$H(t,\theta)=\left(\frac{2}{\sqrt{\pi}}\right)\gamma\left[\frac{3}{2},\frac{t^2}{2\theta^2}\right];\theta>0,t>0, \tag{1}$$

$$h(t,\theta)=\sqrt{\frac{2}{\pi}}\theta^{-3}t^2e^{-\frac{t^2}{2\theta^2}};\theta>0,t>0. \tag{2}$$

where t represents the realization of a random variable following a Maxwell distribution, γ refers to the incomplete gamma function, and θ serves as a distributional parameter. Probability density and probability distribution functions are mathematical expressions that describe the likelihood of a random variable taking on a specific value or falling within a certain range. These functions provide valuable information about the behavior and characteristics of a random variable, enabling us to make predictions and analyze data in various fields. The probability of a variable being less than or equal to a certain value is represented by the DF, whereas the PDF represents the probability that the variable falls within a particular range. The scale parameter, denoted by θ, represents a scaling factor that produces various density curves for the Maxwell distribution when different values are assigned. Fig. 1 displays graphical representations of the PDF and DF for a Maxwellian random variable, highlighting variations in the θ parameter.

The Maxwell distribution density curves are asymmetric and right skewed, especially for smaller values of the scale parameter θ, as shown in Fig. 1(a). As θ increases, the skewness of the Maxwell distribution decreases, moving the curve toward symmetry. Fig. 1(b), on the other

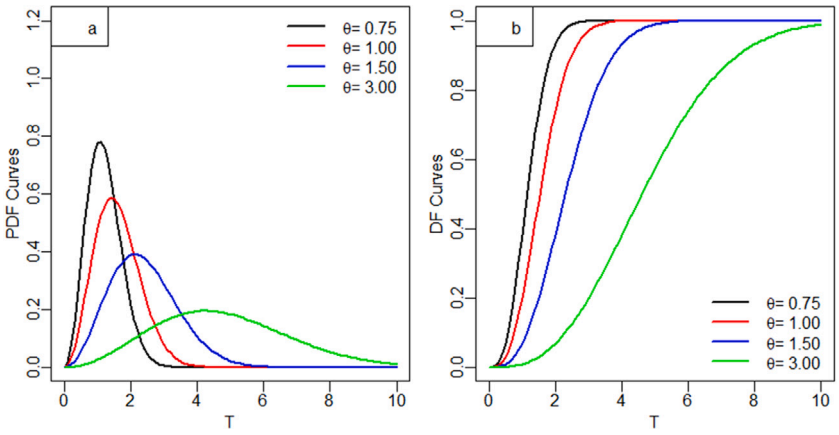

Fig. 1. Maxwell model at different scaling factor values: (a) probability density and (b) distribution function.

hand, shows that the DF is right-continuous, constantly growing, and falls between 0 and 1. The Maxwell density model belongs to the family of Maxwell densities and includes mixed Maxwell distributions. The Maxwell distribution was initially established and used to characterize the velocities of particles in ideal gases. The parameter of the Maxwell distribution is often estimated via the maximum likelihood (ML) method, which has been used in the vast majority of investigations. Consider a random sample of n observations from the Maxwell model, $t_1, t_2, \ldots, t_n$. The ML-based point estimator is defined as follows:

$$\hat{\theta}^2 = \frac{\sum_{j=1}^{n} t_j^2}{3n} \tag{3}$$

The design of the V chart relies on the statistical properties of the estimator, as presented in Eq. (3), with the key feature that $\hat{\theta}^2$ is an unbiased estimator of θ^2. By utilizing the desirable properties of the sampling distribution of the plotting statistic, the structure of the V chart for in-control (IC) θ^2 is given by:

$$\begin{aligned} \text{LCL} &= \theta^2 - k\sqrt{\frac{2\theta^4}{3n}} \\ \text{UCL} &= \theta^2 + k\sqrt{\frac{2\theta^4}{3n}} \end{aligned} \tag{4}$$

The designed limits of the V chart defined in Eq. (4) are known as k-sigma limits, where the constant k is determined as the quantile of the gamma model, which is selected on the basis of a predefined value for the false alarm rate, denoted as α. The square root of θ^2 is a biased estimator of the scaling factor θ. Additionally, the estimator θ^2 does not estimate the corresponding parameter in the same unit of measure as the observed original quality characteristic. In contrast, V_{SQ} is developed on the basis of the sampling distribution of the positive square root of the statistic given in Eq. (3). The V_{SQ} statistic is defined as follows:

$$V_{\text{SQ}} = \sqrt{\hat{\theta}^2} \tag{5}$$

Eq. (5) can be rewritten as:

$$V_{\text{SQ}} = \frac{\theta}{\sqrt{3n}} U \tag{6}$$

where $U = \sqrt{\sum_{j=1}^{n} t_j{}^2}$ follows the chi-distribution with 3n degrees of freedom (Shah et al., 2021). The MXEWMA chart is based on the V_{SQ} statistic as outlined in Eq. (6). The shape of the V_{SQ} statistic is influenced by the sample size and the scale parameter chosen for the Maxwell distribution. As these two factors are selected, they affect the skewness of the plotting statistic, which remains unless there is a considerable increase in either the scale parameter or sample size. To preserve the skewed curve characteristic of the Maxwell distribution, we select the scale parameter to a lower value when generating our results. Furthermore, in line with practical considerations in SPC, selecting a sample size that is relatively small or moderate, usually ranging from 1 to 10 or 12, is standard practice. This rationale for selecting parameters also aligns with previous work (Saghir et al., 2023). By utilizing the sampling distribution of the square root estimator, we can establish the k-sigma bounds of the V_{SQ} chart as follows:

$$\begin{aligned} \text{LCL} &= \theta T_n - k\theta\sqrt{1 - T_n^2} \\ \text{UCL} &= \theta T_n + k\theta\sqrt{1 - T_n^2} \end{aligned} \tag{7}$$

where the sample-size-dependent function is $T_n = \sqrt{\frac{2}{3n}} \frac{\Gamma\left(\frac{3n+1}{2}\right)}{\Gamma\left(\frac{3n}{2}\right)}$, and the choice of k is made by selecting the quantile of the chi distribution in accordance with a predefined value for the false alarm rate. The scale parameter of Maxwell-distributed systems is routinely tracked via both designs. The V_{SQ} chart outperforms alternative methods in detecting moderate to substantial alterations in the scaling factor. In the following section, we detail the MXEWMA charting approach that may be used to further improve the out-of-control (OOC) performance of the V_{SQ} chart under scenarios of smaller shifts in the investigated parameter.

3. Proposed chart

The design structure of the proposed MXEWMA chart is provided in this section. Let us assume a Maxwell distribution for the quality characteristics of the understudy, as shown in Eq. (1). The Maxwell model with the scale parameter has n realizations, denoted by $t_1, t_2, \ldots, t_n$. Using the statistics of interest, we can define the geometric moving average (GMA) method as follows:

$$Y_j = (1 - \delta)Y_{j-1} + \delta V_{\text{SQ}_j} \quad \text{for } j = 0, 1, \ldots \tag{8}$$

The smoothing constant δ, which falls within the range of zero to one, is a crucial element in determining the interval limit. Additionally, this constant represents the GMA at a specific time. The observations V_{SQ} are recorded in a sequential manner and represent the estimated values obtained by performing calculations for each subgroup. These subgroups are determined on the basis of the designed sampling scheme and their sizes. As with geometric growth, the smoothing weights decrease exponentially. It is common practice to make Y_0 the starting point for tracking. The similarities between Eq. (8) and the geometric progression enable the verification of numerous additional GMA features. To express the realizations Y_j stated in Eq. (8) differently, we can use a moving average of both past and present observations, as follows:

$$\begin{aligned} &Y_0 = \theta_0, \\ &Y_j = (1 - \delta)^j Y_0 + \sum_{i=0}^{j-1} \delta(1 - \delta)^i V_{\text{SQ}}(ji) \end{aligned} \tag{9}$$

where the starting value Y_0 is established as the target value.

Generally, the weight $\delta(1-\delta)^i$ gradually diminishes exponentially as more weight is given to recent observations, whereas older observations have less influence on the overall result. As time progresses, the impact of a value on the plotting statistic exponentially diminishes because of the smoothing process and decay rate. As a result, the model becomes more adaptive and responsive to changes in the data over time. Additionally, a smoothing constant of 1 enables the MXEWMA chart to achieve a conventional design, making it more versatile and adaptable. The proposed MXEWMA uses the following values for Y_j, LCL and UCL for its parameters:

$$\begin{aligned} \text{LCL} &= \theta T_n - kS_{V_{\text{SQ}}}\sqrt{\frac{\delta}{2-\delta}\left[1-(1-\delta)^{2j}\right]} \\ \text{UCL} &= \theta T_n + kS_{V_{\text{SQ}}}\sqrt{\frac{\delta}{2-\delta}\left[1-(1-\delta)^{2j}\right]} \end{aligned} \tag{10}$$

where θT_n and $S_{V_{\text{SQ}}} = \theta\sqrt{1-T_n^2}$ are the average and standard deviation, respectively, of the V_{SQ} statistic and where k is the correction quantity for symmetrically building the proposed chart. Typically, the false alarm rate is used to adjust k.

Eq. (10) can be computed as follows:

$$\begin{aligned} \text{LCL} &= \theta Q_1 \\ \text{UCL} &= \theta Q_2 \end{aligned} \tag{11}$$

where $Q_1 = T_n - kS_{V_{\text{SQ}}}\sqrt{\frac{\delta}{2-\delta}\left[1-(1-\delta)^{2j}\right]}$, and $Q_2 = T_n + kS_{V_{\text{SQ}}}\sqrt{\frac{\delta}{2-\delta}\left[1-(1-\delta)^{2j}\right]}$.

The process is said to be unstable whenever Y_j is outside the control limits of the LCL and UCL, and corrective action should be taken to quickly identify unmanageable conditions. The time-varying limits given in Eq. (10) fluctuate with j as a function of time. When j is large, $1-(1-\delta)^{2j}$ tends to approach one as j decreases. Thus, in the case of a larger j, we can represent the stable form of the control limits as given below:

$$\begin{aligned} \text{LCL} &= \theta T_n - kS_{V_{SQ}}\sqrt{\frac{\delta}{2-\delta}} \\ \text{UCL} &= \theta T_n + kS_{V_{SQ}}\sqrt{\frac{\delta}{2-\delta}} \end{aligned} \tag{12}$$

However, it is highly recommended that the proposed chart be constructed using the exact parameters stated in Eq. (10). Precise limitations enhance the control chart's early warning of off-target conditions following the deployment of the MXEWMA strategy. When an IC state parameter is known, the abovementioned usage is possible. However, in many cases, process parameters are unavailable; thus, a retrospective IC is used to estimate their values.

When considering the estimate of θ, Eq. (11) can be expressed as:

$$\begin{aligned} \text{LCL} &= \hat{\bar{\theta}}Q_1, \\ \text{UCL} &= \hat{\bar{\theta}}Q_2. \end{aligned} \tag{13}$$

where $\hat{\bar{\theta}} = \frac{\sum_{i=1}^{M}\hat{V}_{\text{SQ}_i}}{M}$ and M represent the overall count of available samples.

Monte Carlo simulation may be used to determine the multiplier k. The Monte Carlo simulation is run with a scale factor θ equal to 0.75, and the data are generated via a sampling distribution that is based on the V_{SQ} statistic. The simulation is conducted until the target IC ARL (ARL_0) is reached. In this simulation, we follow an iterative procedure, as explained by Horng Shiau and Ya-Chen (2005), to find the value of k for target $ARL_0 = 370$. We calculate the values of k for various values of δ and n. Table 1 presents the values of k that can be used to calculate Q_1 and Q_2 to estimate the width of the proposed chart.

Table 1 displays the estimated values for factor k on the basis of 10^5 randomized statistical simulations to generate an approximation of the desired ARL_0 value. The k factor determines the width of the control limits in the MXEWMA chart. The results in Table 1 show that the factor

Table 1
Factor k computed values for the MXEWMA chart.

Sample size	$ARL_0 = 370$				
	δ = 0.05	δ = 0.15	δ = 0.30	δ = 0.60	δ = 0.80
2	2.826	2.827	2.936	3.032	3.063
3	2.702	2.817	2.928	2.997	3.029
4	2.639	2.806	2.928	2.999	3.021
5	2.614	2.816	2.933	2.999	3.012
6	2.605	2.811	2.925	2.990	3.006
8	2.574	2.806	2.929	2.990	3.003
10	2.568	2.809	2.937	2.988	2.999
12	2.564	2.809	2.926	2.987	2.996

Table 2
Components Q_1 and Q_2 for the MXEWMA chart with $\delta = 0.05$.

Time point	Sampling size					
	2		5		8	
	Q_1	Q_2	Q_1	Q_2	Q_1	Q_2
1	0.9195	0.9992	0.9598	1.0071	0.9602	1.0068
2	0.9043	1.0144	0.9509	1.0161	0.9514	1.0156
3	0.8937	1.0251	0.9445	1.0225	0.9451	1.0219
4	0.8853	1.0334	0.9395	1.0274	0.9402	1.0268
5	0.8785	1.0402	0.9355	1.0315	0.9362	1.0307
6	0.8728	1.0459	0.9321	1.0348	0.9329	1.0341
7	0.868	1.0508	0.9293	1.0377	0.9301	1.0369
8	0.8638	1.0549	0.9268	1.0402	0.9277	1.0393
9	0.8602	1.0585	0.9247	1.0423	0.9256	1.0414
10	0.8571	1.0616	0.9228	1.0442	0.9237	1.0432
11	0.8544	1.0644	0.9212	1.0458	0.9221	1.0448
12	0.8519	1.0668	0.9197	1.0472	0.9207	1.0463

Table 3
Components Q_1 and Q_2 for the MXEWMA chart with $\delta = 0.15$.

Time point	Sampling size					
	2		5		8	
	Q_1	Q_2	Q_1	Q_2	Q_1	Q_2
1	0.9195	0.9993	0.907	1.0599	0.9292	1.0501
2	0.9044	1.0144	0.8831	1.0838	0.9103	1.0689
3	0.8936	1.0251	0.8689	1.098	0.8991	1.0802
4	0.8853	1.0335	0.8597	1.1073	0.8918	1.0875
5	0.8785	1.0403	0.8534	1.1135	0.8868	1.0924
6	0.8728	1.046	0.8491	1.1179	0.8834	1.0959
7	0.8679	1.0508	0.846	1.121	0.881	1.0983
8	0.8638	1.0549	0.8438	1.1231	0.8793	1.1
9	0.8602	1.0585	0.8423	1.1247	0.878	1.1012
10	0.8571	1.0617	0.8412	1.1258	0.8772	1.1021
11	0.8543	1.0644	0.8404	1.1266	0.8765	1.1027
12	0.8519	1.0668	0.8398	1.1271	0.8761	1.1032

Table 4
Components Q_1 and Q_2 for the MXEWMA chart with $\delta = 0.60$.

Time point	Sampling size					
	2		5		8	
	Q_1	Q_2	Q_1	Q_2	Q_1	Q_2
1	0.4461	1.4727	0.6578	1.3092	0.7321	1.2472
2	0.4065	1.5122	0.6327	1.3343	0.7122	1.267
3	0.4005	1.5183	0.6289	1.3381	0.7092	1.2701
4	0.3995	1.5192	0.6282	1.3387	0.7087	1.2706
5	0.3993	1.5194	0.6281	1.3388	0.7086	1.2706
6	0.3993	1.5194	0.6281	1.3388	0.7086	1.2707
7	0.3993	1.5194	0.6281	1.3388	0.7086	1.2707
8	0.3993	1.5194	0.6281	1.3388	0.7086	1.2707
9	0.3993	1.5194	0.6281	1.3388	0.7086	1.2707
10	0.3993	1.5194	0.6281	1.3388	0.7086	1.2707
11	0.3993	1.5194	0.6281	1.3388	0.7086	1.2707
12	0.3993	1.5194	0.6281	1.3388	0.7086	1.2707

Table 5
Components Q_1 and Q_2 for the MXEWMA chart with $\delta = 0.80$.

Time point	Sampling size					
	2		5		8	
	Q_1	Q_2	Q_1	Q_2	Q_1	Q_2
1	0.268	1.6508	0.5474	1.4196	0.6447	1.3345
2	0.2543	1.6645	0.5387	1.4283	0.6379	1.3414
3	0.2537	1.665	0.5384	1.4286	0.6376	1.3417
4	0.2537	1.665	0.5384	1.4286	0.6376	1.3417
5	0.2537	1.665	0.5384	1.4286	0.6376	1.3417
6	0.2537	1.665	0.5384	1.4286	0.6376	1.3417
7	0.2537	1.665	0.5384	1.4286	0.6376	1.3417
8	0.2537	1.665	0.5384	1.4286	0.6376	1.3417
9	0.2537	1.665	0.5384	1.4286	0.6376	1.3417
10	0.2537	1.665	0.5384	1.4286	0.6376	1.3417
11	0.2537	1.665	0.5384	1.4286	0.6376	1.3417
12	0.2537	1.665	0.5384	1.4286	0.6376	1.3417

k varies on the basis of sample size values and the smoothing constant δ. The choice of n and δ depends on the specific monitoring needs. Typically, smaller sample sizes have relatively higher k values than do larger sample sizes for a fixed value of δ. This indicates that there is more uncertainty with smaller sample sizes. As the sample size increases, the control limits narrow due to lower k values, indicating that the results from larger sample sizes are more statistically reliable. Moreover, as the value of the smoothing constant increases, the corresponding k values also increase, indicating the need for wider control limits to maintain the desired ARL_0 of 370. Tables 2–5 describe how the components Q_1 and Q_2, which determine the control limits, are influenced by the weighting parameter δ, sample size n, and time point j. When δ is small, as shown in Tables 2–3, the time-varying limits given in Eq. (10) take a longer time to converge to stable limits, as described in Eq. (12). This results in a steady increase in the values of Q_1 and Q_2 as time point j increases. When the weighting constant δ is relatively large, as shown in Tables 4–5, the time-varying limits quickly converge to stable limits regardless of the sample size. The computational work of the suggested chart may be simplified by using the coefficients Q_1 and Q_2 shown in Tables 2–5; thus, the adjustment factor k is not necessary for building control limits.

4. Performance evaluation

Here, we provide the features of the RL distribution that are used to evaluate the proposed chart's statistical efficacy. To test how well the MXEWMA chart works, large-scale simulations are run. Let us view this case in the hypothesis testing framework, assuming that the DGP is in the IC state. The goal is to determine whether there is sufficient evidence to conclude that the process is still IC. If the likelihood is sufficiently low, we reject the null hypothesis and conclude that there is evidence to suggest that the process is no longer in control. Owing to the control limits being utilized as decision-making benchmarks and considering the inherent randomness in observed data, the MXEWMA chart could falsely indicate changes in the process distribution. In hypothesis testing, this is known as a type I error. Therefore, it is important to note whether the process's IC state shifts as a means of testing the hypothesis. Our working hypotheses are as follows:

$H_0 : \theta = \theta_0$; i.e., the system is IC at θ_0

$H_1 : \theta = \theta_1$; i.e., the system is OOC at θ_1

The RL comprises samples collected from the initial point of evaluation until a signal indicating an OOC state is detected within the process. Since the RL profile is established by observing samples, which are believed to be unrelated and uniformly distributed in time and space, the RL is a random variable. The average RL, sometimes abbreviated ARL, is determined for both the IC state, represented by ARL_0, and the OOC state, designated by ARL_1. While a small ARL_1 value and a large ARL_0 value would be ideal for any given control chart, these conditions are often somewhat difficult to achieve. To reach an acceptable middle ground, followers of the theory of control charts often set the ARL_0 value to a predetermined threshold and strive to minimize the ARL_1 value. The following is an approximate formula for calculating the ARL value via Monte Carlo simulation:

$$\mathrm{ARL} = \frac{\sum_{j=1}^{N} \mathrm{RL}_j}{N} \tag{14}$$

where N is the total number of simulated runs and where RL_j is the run length of the jth run. In the simulation setup, the following algorithm is utilized to determine the estimated ARL and its related metrics for the MXEWMA chart:

Step 1: Define the input values n, θ, δ, ARL_0, ε, and N and specify the change point $\tau > 1$ in the case of steady-state performance.

Step 2: Initialize the process by setting $Y_0 = \theta_0$ at $j = 1$.

Step 3: Generate a random sample of size n of the V_{SQ} statistic via Eq. (6) and calculate the MXEWMA plotting statistic Y_j according to Eq. (8).

Step 4: If $\left|Y_j\right| > CL$, return RL = j; otherwise, increment j by 1 and repeat Step 3.

Step 5: Iterate through Steps 2–4 a total of N times to acquire N run lengths.

Step 6: Obtain the ARL via Eq. (14).

To approximate the distribution of RL for the MXEWMA chart, we utilized 10^5 iterations in this simulation setup. Owing to the substantial variation in the assumed Maxwell data, characterized by a high degree of skewness, the implementation of the ARL as an assessment measure might not be suitable. We also considered the median and standard deviation of the RL random variable as performance indicators since the ARL metric might lead to erroneous interpretations. Hence, to obtain a more comprehensive evaluation of the chart's performance, it is important to analyze additional percentiles, such as the median RL (MRL). This approach provides a better understanding of how the chart performs in different scenarios. The MRL could be a favorable measure from the perspective of robustness. This preference arises from the notable right-skewed nature of the RL distribution, as discussed earlier. Using a simulation approach and setting the IC scale parameter to a value of 0.75, we calculate the values of the assessment measures for various IC and OOC situations of the Maxwell process. Tables 6–7 provide the computed ARL values for a given smoothing constant.

The results of the performance metrics of the MXEWMA under a wide variety of scale parameter changes are shown in Table 6. The ARL for the IC state process is shown to be consistently close to the predetermined value of ARL_0 across all sample sizes. The MRL in the IC state is also consistently approximately 254–260, showing robustness to some degree in the chart's central tendency. Additionally, the $SDRL$ values in the IC state are relatively high for smaller sample sizes (e.g., n = 2), indicating more variability in the chart's performance when the sample size is small. As the sample size increases, $SDRL$ decreases, demonstrating more stable performance. In contrast, ARL, MRL and $SDRL$ for the OOC state decrease steadily as the shifting parameter increases. For example, for sample sizes of 2, 6, and 10, the associated ARL values for detecting a 20% increase in the scaling parameter are decreased to approximately 12, 5, and 3, respectively. However, for sample sizes of 2, 6, and 10, the corresponding decreases in MRL are approximately 8, 3, and 2, respectively. The $SDRL$ values also decrease with ARL, reflecting that the chart becomes more consistent in its detection as the process shifts further to the OOC state. The same patterns of behavior are shown for the same range of small changes in the scale parameters, as discussed above with respect to Table 7. Moreover, the findings presented in Tables 6–7 stem from the zero-state performance of the MXEWMA chart. The zero-state assessment assumes that the phase II process under monitoring initiates from an OOC state at a specific initial point. However, in real-world scenarios, we cannot

Table 6
The outcomes of the MXEWMA scheme at the specified value of $ARL_0 = 370$.

Shifting parameter	$\delta = 0.15$								
	$n = 2$			$n = 6$			$n = 10$		
	MRL	ARL	SDRL	MRL	ARL	SDRL	MRL	ARL	SDRL
1.00	261.39	371.61	371.25	256.12	369.95	369.55	255.81	370.05	369.75
1.02	168.26	243.25	242.75	133.27	192.77	192.27	107.66	155.82	155.32
1.04	101.43	146.84	146.34	61.48	89.2	88.7	42.14	61.29	60.79
1.06	63.03	91.43	90.93	31.09	45.35	44.85	20.48	30.05	29.55
1.10	28.99	42.33	41.83	11.86	17.61	17.10	7.70	11.62	11.11
1.20	8.00	12.05	11.54	3.24	5.19	4.66	2.11	3.57	3.03
1.30	3.80	6.00	5.48	1.53	2.74	2.18	1.00	2.00	1.41
1.40	2.28	3.81	3.27	0.91	1.87	1.28	0.58	1.44	0.80
1.50	1.54	2.76	2.20	0.62	1.48	0.84	0.39	1.2	0.49
1.60	1.14	2.20	1.62	0.45	1.27	0.59	0.28	1.09	0.31
1.70	0.90	1.86	1.26	0.35	1.16	0.43	0.21	1.04	0.20
1.80	0.73	1.63	1.01	0.28	1.09	0.31	0.15	1.01	0.10

Table 7
The outcomes of the MXEWMA scheme at the specified value of $ARL_0 = 370$.

Shifting parameter	$\delta = 0.30$								
	$n = 2$			$n = 6$			$n = 10$		
	MRL	ARL	SDRL	MRL	ARL	SDRL	MRL	ARL	SDRL
1.00	258.18	372.97	372.47	256.07	369.92	369.43	256.18	370.09	369.59
1.02	168.57	243.69	243.19	144.08	208.36	207.86	130.36	188.57	188.07
1.04	110.09	159.33	158.83	75.56	109.51	109.01	57.92	84.06	83.56
1.06	73.42	106.43	105.93	42.07	61.2	60.7	28.97	42.29	41.79
1.10	36.13	52.62	52.12	16.27	23.98	23.47	10.36	15.45	14.94
1.20	10.58	15.77	15.26	4.00	6.29	5.77	2.56	4.21	3.68
1.30	4.87	7.54	7.02	1.89	3.26	2.71	1.20	2.28	1.71
1.40	2.90	4.71	4.18	1.09	2.13	1.55	0.7	1.59	0.97
1.50	1.97	3.37	2.83	0.74	1.64	1.02	0.46	1.28	0.60
1.60	1.46	2.64	2.08	0.55	1.39	0.74	0.33	1.14	0.40
1.70	1.14	2.19	1.61	0.41	1.23	0.53	0.24	1.06	0.25
1.80	0.93	1.90	1.31	0.33	1.14	0.40	0.20	1.03	0.18

overlook the steady-state performance. Under the steady-state scenario, the process remains in an IC state for a long period before transitioning to the OOC state at random points in time. The steady-state RL for the proposed model can be defined as:

$$RL_{ss} = \min\left\{ j \geq \tau \,\middle|\, V_{SQj} \langle LCL \text{ or } V_{SQj} \rangle UCL \right\}; \quad \tau = 1, 2, \ldots \tag{15}$$

where $\tau = 1$ denotes the number of IC samples observed before a shift occurs in the scale parameter of the Maxwell process, with $\tau = 1$ indicating a zero-state RL.

Usually, the index τ in Eq. (15) represents the change point utilized in the following change point model (Knoth, 2021):

$$\theta_j = \begin{cases} \theta_0, & \text{if } j < \tau \\ \theta_1, & \text{if } j \geq \tau \end{cases} \tag{16}$$

where $\theta_1 = \varepsilon\theta_0$ represents the value at the OOC state with a ε change in the scale parameter of the Maxwell process. The average steady-state RL for the proposed chart in a simulation setup can subsequently be computed via Eq. (15). Therefore, Eq. (15) in the steady-state case denotes a type of conditional expected RL, implying that a change in monitoring parameters occurs at subgroup number $\tau = 1, 2, \ldots$, given that no false alarm has been raised. The steady-state ARL can be calculated for different change points τ across varying combinations of n, δ and ARL_0. The steady-state performance of the MXEWMA chart for a delay of 100 (i.e., $\tau = 100$) samples for varying shifts compared with zero-state ARL is depicted in Fig. 2.

Fig. 2 shows the OOC run-length characteristics of the MXEWMA chart for both the zero-state and steady-state scenarios. It is evident from Fig. 2 that when selecting the MXEWMA chart with comparable zero-state ARL properties, the corresponding steady-state ARL performances are similar for both smaller and larger values of δ. Notably, the ARL computation in Fig. 2 is conducted for both zero-state and steady-state scenarios with a 100th sample delay detection. However, comparable outcomes persist across various values of τ.

5. Simulation analysis

In this section, we describe the implementation of the MXEWMA scheme and its usefulness in identifying minute incremental alterations in target parameters via simulated data. The effectiveness of the MXEWMA chart in identifying minor changes is verified by simulated data.

The steps involved in constructing control limits for the MXEWMA chart on the basis of simulated data are listed below:
Step 1. Select the input values n, θ, δ, ARL_0 and ε.
Step 2. Initialize by setting $Y_0 = \theta_0$ at $j = 1$.
Step 3. Generate a random sample of size n of the V_{SQ} statistic via Eq. (6) and calculate the MXEWMA plotting statistic Y_j according to Eq. (8).
Step 4. Repeat Steps 1–3 until the desired sample size is achieved.
Step 5. Choose the multiplier k from Table 1 for given values of δ and n.
Step 6. The control limits are calculated according to Eq. (9).
Step 7. The estimated MXEWMA statistics Y_j are plotted against the constructed limits.

Notably, to ensure consistent outcomes for both the V_{SQ} chart and the MXEWMA chart, the same seed is employed with the random number generator. We use the VGAM package in R to produce a randomly selected sample of 20 values from a Maxwell model with a scaling factor of $\theta = 0.75$. Fig. 3 displays these 20 measurements on a standard Shewhart-type V_{SQ} chart with parameters $ARL_0 = 370$ and $n = 8$, as well as a suggested chart with $ARL_0 = 370$, $n = 8$ and $\delta = 0.15$. As shown in Fig. 3, all the points fall within the acceptable range, revealing that the underlying process is under statistical control. Ten new values are drawn at random from the Maxwell distribution; however, the scale parameter values used are $\theta = 0.90$ and $\theta = 0.94$, which indicate that a 20% and 25% (i.e., $\varepsilon = 1.2$ and $\varepsilon = 1.25$) increase over the target value, respectively, to test the control chart's sensitivity

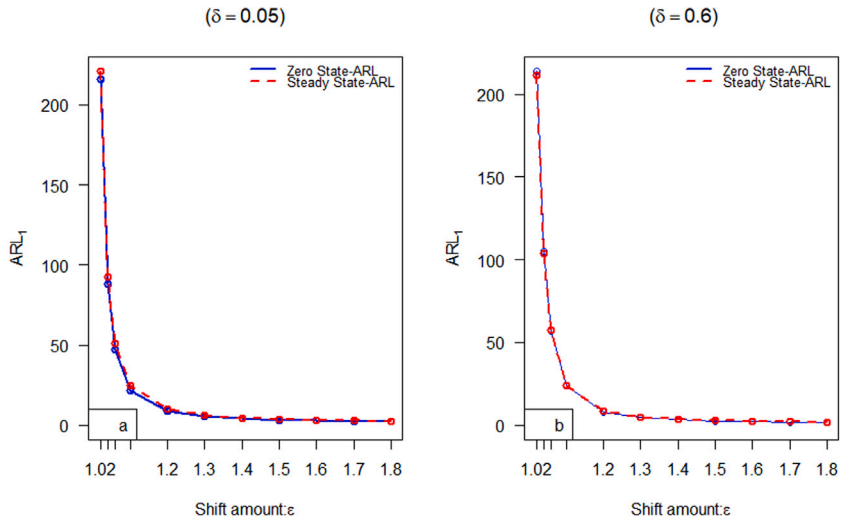

Fig. 2. Comparative performance of the MXEWMA chart in the zero-state and steady-state cases at $n = 5$ and 370.

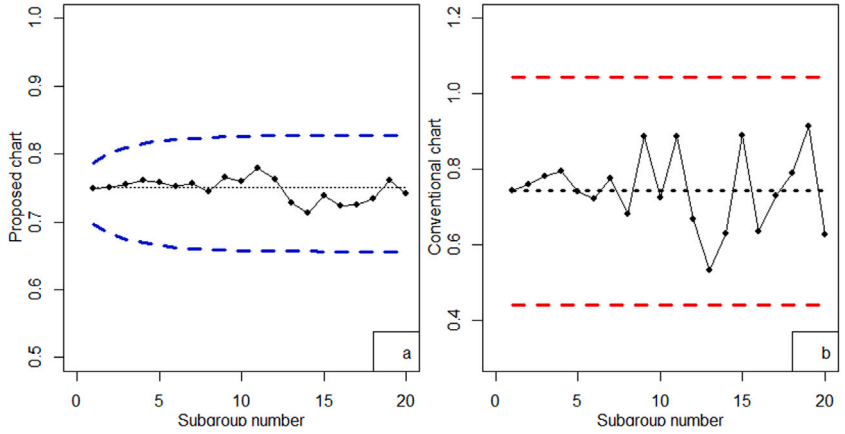

Fig. 3. The proposed MXEWMA scheme and V_{SQ} scheme for simulated data.

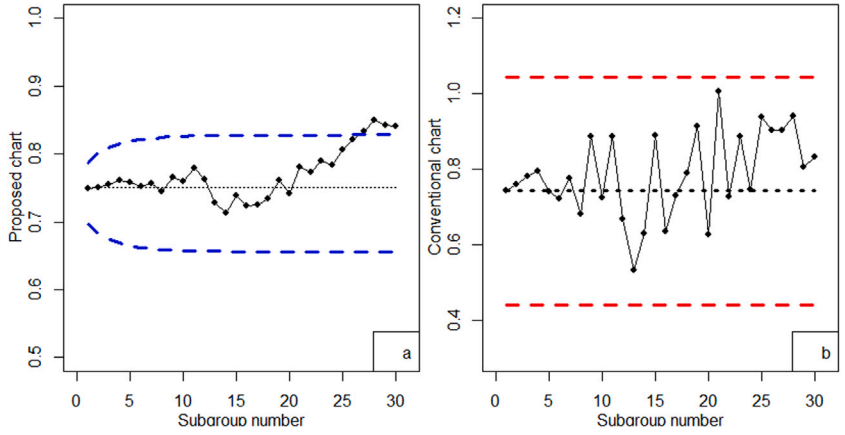

Fig. 4. The proposed MXEWMA scheme and V_{SQ} scheme for simulated data with a 20% increase in the target parameter.

to detecting shifts. Since the process has already exhibited a change of 20% and 25% in the observed parameter θ, these ten values can be regarded as samples from a phase of the process that is in the OOC state. Fig. 4 and Fig. 5 indicate that the process is under OOC conditions. This is evident from the data points falling outside the control limits in Figs. 4 and 5. The presence of abnormal patterns suggests that the process is not operating within its expected range of variation.

In Fig. 4(a), beyond the 20th data point, all subsequent values exhibit an upward trend and are positioned above the central line, suggesting that the process is in an OOC state. In contrast, in Fig. 4(b), the conventional V_{SQ} chart continues to reflect the IC state of the process, and it is not sensitive enough to detect a slight shift in the studied parameter. A sudden shift in the target parameter is also detected by the MXEWMA, as shown in Fig. 5(a). On the other hand, the process

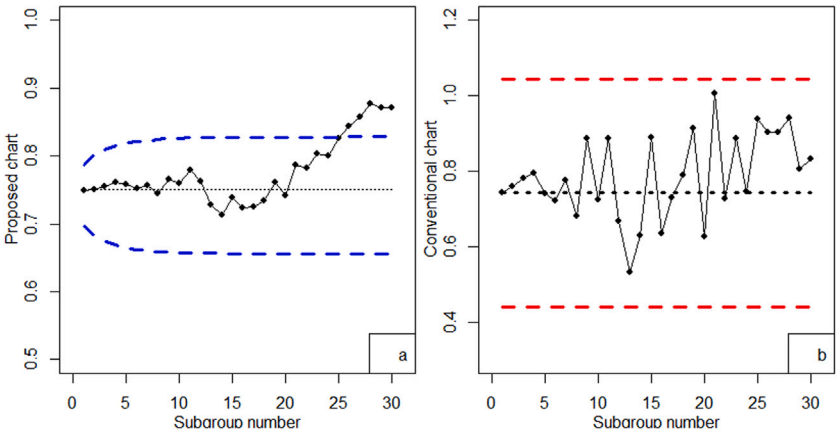

Fig. 5. The proposed MXEWMA scheme and V_{SQ} scheme for simulated data with a 25% increase in the target parameter.

is indeed OOC after the 20th sample, but the V_{SQ} chart (see Fig. 5(b)) does not provide better proof of this fact. This inability to detect the shift can be attributed to the relatively modest amount of change in the target parameter.

6. Comparative analysis

In this section, we assess the performance of our suggested MXEWMA chart in comparison to traditional charts for Maxwell quality characteristics, particularly emphasizing power curves. The V_{SQ} chart and VEWMA chart are two prevalent control charts designed on the basis of the Maxwell distribution assumption. In the framework of control charts, this comparison provides insight into the probability of either rejecting a batch of subpar quality or permitting a workflow to continue operating if it meets the desired performance levels in relation to a specific quality attribute. In simpler terms, "power" refers to the probability of correctly identifying that a process is not in an IC state when it is actually in an OOC state. Power is a critical measure in hypothesis testing because it quantifies the ability of a control chart to detect deviations from the IC state and to identify when a process is not operating within acceptable limits. Analyzing the usefulness of a control chart is often more practical when its power is considered, which can be defined as follows:

$$\text{Power} = 1 - \beta = \text{Prob}\{\text{Reject null hypothesis}|\text{Null hypothesis is false}\} \tag{17}$$

where β is the type II error, which is also sometimes referred to as the risk to the consumer in the SPC literature. The value of β depends on the size of the sample, with a lower value predicted for larger sample sizes.

To maintain a consistent comparative framework across the proposed chart, VEWMA chart, and VSQ chart, it was presumed that the data adhered to the Maxwell distribution with a scale parameter $\theta = 0.75$. Using the simulation procedure outlined in Section 4, we conducted 10^5 Monte Carlo simulations to analyze the power profiles for the proposed and existing control charts comprehensively. The MXEWMA chart and the V_{SQ} chart's power curves (PCs) were calculated for a range of n values and $ARL_0 = 370$ via the specified expressions provided in Eqs. (7) and (10). Fig. 6 displays the results of comparing the proposed chart's PCs with those of the VEWMA chart and the V_{SQ} chart using a smoothing constant $\delta = 0.30$. Fig. 6 shows that the MXEWMA chart has the highest power across all δ values, indicating its superior ability to detect process shifts of different magnitudes compared with the V_{SQ} chart and VEWMA chart. When the shift constant is set to 1, indicating that the underlying workflow is in an IC state (as shown by the PCs in Fig. 6), the three charts exhibit identical behavior. In the IC state, the power provided by these three charts is most in line with the assumed value of α (i.e., $\alpha = 0.0027$), which gives $ARL_0 = 370$. All control charts show an increase in strength when the process deviates from the set point. As the sample size increases, all three control chart methods exhibit enhanced sensitivity to process changes, as indicated by the overall increase in power across different δ values. However, the superior performance of MXEWMA in detecting process shifts remained evident across all sample sizes. The proposed chart has greater power than the V_{SQ} and VEWMA charts do. For example, the proposed chart provides powers of approximately 0.133, 0.262, and 0.407 for detecting shifts of 20%, 30%, and 50% in θ at $n = 5$, respectively. In contrast, the V_{SQ} and VEWMA charts only have powers of 0.012, 0.028, and 0.054 and 0.035, 0.073, and 0.118, respectively, at the same shift levels. With respect to identifying a much greater change, the V_{SQ} chart is just as effective as the proposed chart. These graphs continue to emphasize the superior performance of the MXEWMA chart in detecting process shifts, making it a promising choice for various real-world applications.

7. Estimation effect on the MXEWMA chart

In Section 4, the performance of the proposed MXEWMA chart was examined under the assumption that the parameters of the Maxwell distribution are known. However, in practice, the parameters are seldom known and estimated from Phase I samples (m), which is known as retrospective analysis (Jensen et al., 2006). The parameter estimation of parameter (s) has a significant effect on the Phase-II performance of a control chart (see Abbas, 2018; Abbas et al., 2020; Alevizakos et al., 2023; Jensen et al., 2006; Jones-Farmer et al., 2014; Saghir, Abbasi et al., 2021). This section investigates the impact of parameter estimation on the IC performance of the MXEWMA chart. The control limits of the proposed chart under the estimated parameter can be determined via Eq. (13). For the analysis, a charting constant of $ARL_0 = 370$ is considered in the computation procedure. The results reported in Table 8 are based on sample sizes $n \in \{4, 8\}$, weighting constants $\delta \in \{0.15, 0.30, 0.60\}$ and subgroup sizes $m \in \{25, 50, 100, 200, 400\}$.

Table 8 clearly shows that the performance indicators of the proposed MXEWMA chart with the estimated parameters approach their nominal values as the subgroup size increases. This indicates that when the parameter is unknown, larger subgroup sizes are required at each weighting constant to achieve the desired nominal value of ARL_0. It is also evident from Table 8 that the IC performance of the proposed MXEWMA chart is significantly affected by m because of practitioner-to-practitioner variation. The design of the proposed MXEWMA chart can be adjusted to capture this practitioner variation by following the method of Saghir, Abbasi et al. (2021). However, this requires a separate study and is not the focus of the current work.

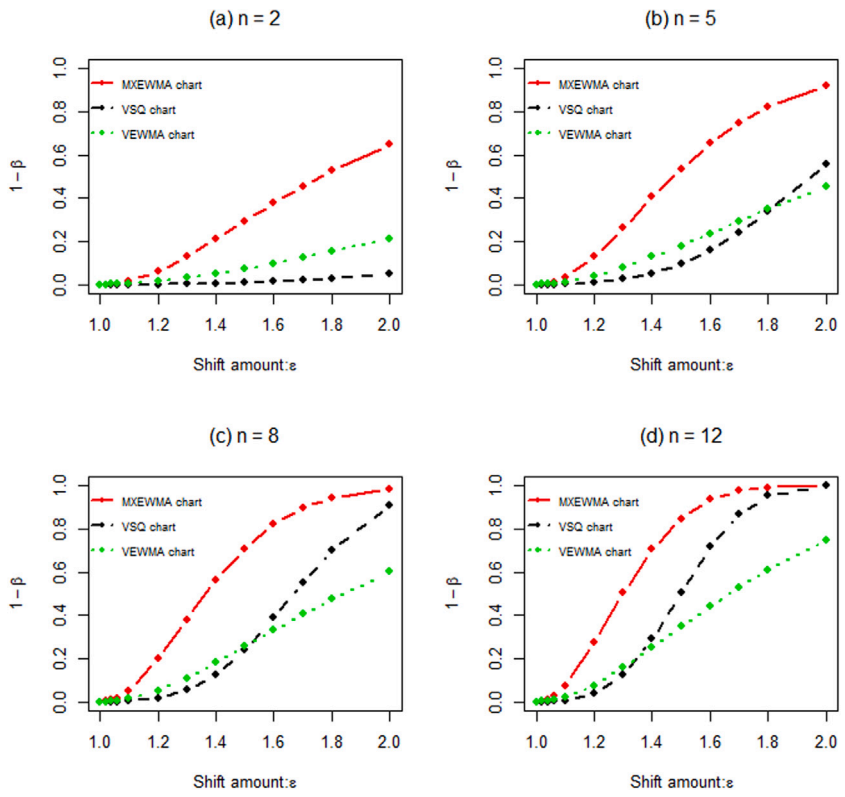

Fig. 6. Power curves of the proposed chart, VEWMA chart and V_{SQ} chart.

Table 8
Estimation effect on IC run length characteristics of the MXEWMA chart.

δ	m	$n = 4$			$n = 8$		
		ARL0	MRL	SDRL	ARL0	MRL	SDRL
0.15	25	42.89	29.38	42.39	88.84	60.84	87.77
	50	87.24	60.12	86.74	161.48	111.58	160.98
	100	116.67	111.71	161.17	263.29	182.15	262.79
	200	262.06	181.30	261.56	342.52	236.07	342.02
	400	337.12	233.33	336.62	362.85	251.16	362.35
0.30	25	45.65	31.29	45.15	91.41	63.01	90.91
	50	90.95	62.69	90.45	164.07	113.38	163.57
	100	162.47	112.27	161.97	270.96	187.47	270.46
	200	269.65	186.56	269.15	349.12	241.64	348.62
	400	345.75	239.31	345.25	370.56	256.56	370.14
0.60	25	45.45	31.16	44.95	91.81	63.29	91.31
	50	93.13	64.21	92.63	162.79	112.49	162.29
	100	166.00	114.72	165.50	269.98	186.79	269.48
	200	266.96	184.70	266.46	347.47	240.50	346.97
	400	345.71	239.21	345.21	370.81	256.37	370.31

8. Real data application

To demonstrate the effectiveness and practicality of the MXEWMA control chart, real-life data related to the aerospace industry are discussed in this section. We implemented the proposed MEWMA scheme on aircraft windshield failure data. The data were initially used for reliability analysis and prediction of warranty costs, with detailed information provided by Murthy et al. (2004). A brief description of aircraft windshields and their inspection is depicted in Fig. 7. Fig. 7 is taken from the second source for illustration purposes.

The windshield of a large aircraft is a critical component that is composed of several layers of materials, all laminated under high temperature and pressure (Lu et al., 2024). Windshields are exposed to multiple and sometimes intense stresses during flight, particularly during take-off and landing. Failures typically manifest as damage to the outer layer, malfunction of the heating mechanism, or degradation, such as partial delamination, necessitating replacement. In the domain of reliability studies, one of the key challenges in handling reliability data is determining an appropriate failure distribution. As a result, these data have been employed in multiple studies to aid in developing statistical models for reliability analysis (Elshahhat et al., 2023; Ruhi et al., 2015). Ensuring optimal pilot visibility is crucial for the safe operation of an aircraft. In recent years, aircraft manufacturers and operators have implemented different measures to maintain clear vision through transparent areas. Consequently, aerospace glass manufacturers are continuously gathering and assessing data on windshields to enhance the design, quality control, and operational protocols for satisfactory performance under various aircraft environmental conditions. The dataset consists of 84 measurements of the failure times of windshields that failed at the time of observation. Fig. 8 displays a dot plot of the windshield failure data, providing a clear visual representation to identify outliers and recognize potential patterns of randomness in the individual values. A dot plot can be an effective tool for data visualization, enhancing data analysis and decision-making processes (Abbas et al., 2020; Abbas, Nazir et al., 2024). To ensure accuracy, it is crucial to visually evaluate whether a single-parameter Maxwell model is an appropriate representation of failure time data before proceeding with further analysis. Our hypothesis suggests that failure measurements can be effectively described via the Maxwell model. Probability plotting, a graphical method, provides a strong means of evaluating how well sample data align with a hypothesized distribution. To identify the most suitable distribution for data generation, a subjective visual examination of the data is adopted in this approach. For our analysis, we utilized the Fitdistplus package in R to create an empirical distribution and generate essential probability plots, as shown in Fig. 9. These visualizations offer valuable insights into how well our data align with the Maxwell distribution, enabling us to make informed decisions for modeling purposes.

A careful examination of the deviations observed in Fig. 9 clearly reveals that a Maxwell distribution could be an appropriate model



Fig. 7. Commercial aircraft windshield market (Facility Supplier for Aircraft Company, 2023).

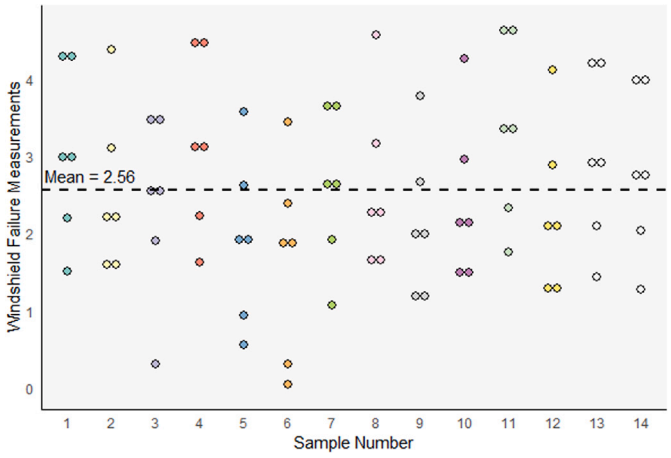

Fig. 8. Dot plot of the failure times of aircraft windshields.

Table 9
Windshield failure measurements and plotting statistic.

Sample no	Observations						V_{SQj}
	I	II	III	IV	V	VI	
1	2.964	4.274	1.506	2.19	3.00	4.305	1.851
2	1.568	2.194	3.103	4.376	1.615	2.223	1.556
3	2.481	3.467	0.309	1.899	2.61	3.478	1.505
4	3.114	4.449	1.619	2.224	3.117	4.485	1.927
5	0.557	1.911	2.625	3.578	0.943	1.912	1.251
6	0.04	1.866	2.385	3.443	0.301	1.876	1.169
7	2.632	3.595	1.07	1.914	2.646	3.699	1.587
8	1.652	2.229	3.166	4.57	1.652	2.3	1.609
9	1.124	1.981	2.661	3.779	1.248	2.01	1.336
10	1.48	2.135	2.962	4.255	1.505	2.154	1.5
11	3.344	4.602	1.757	2.324	3.376	4.663	2.027
12	1.281	2.085	2.89	4.121	1.303	2.089	1.441
13	2.902	4.167	1.432	2.097	2.934	4.24	1.807
14	2.688	3.924	1.281	2.038	2.823	4.035	1.71

for windshield failure data. To delve deeper into this hypothesis, we employ the Kolmogorov–Smirnov (KS) test, which provides a formal measure of goodness-of-fit. By combining both graphical analysis and statistical testing, we aim to gain a comprehensive understanding of the suitability of the Maxwell distribution for our data. The KS test provides a p value of 0.856 for the failure data, indicating that the Maxwell model is somewhat suitable for our data. Thus, we can utilize aircraft windshield failure data as an example case to demonstrate the application of the MXEWMA chart.

Importantly, although other statistical models may be more suitable for this dataset, our main goal is to demonstrate how the methodology can be applied to monitoring data that are slightly skewed and do not perfectly fit the model. To illustrate our control chart monitoring approach, we divided a dataset with 84 observations into fourteen subgroups, with each subgroup containing six observations. These subgroups are presented in Table 9.

The final column of Table 9 contains the meticulously recorded preliminary sample statistics according to Eq. (5). By referring to Table 1, we can determine a suitable smoothing constant, denoted as δ, for a subgroup sample size of 6. According to In Table 1, $\delta = 0.30$ corresponds to the critical value $k = 2.925$. Subsequently, we can utilize the critical value k to compute the UCL and LCL, as outlined in Eq. (10). The parameters of the proposed monitoring scheme are depicted in Fig. 9 to ensure that any deviation from the expected value is readily identifiable (see Table 9).

The plotting statistic V_{SQj} in Fig. 10 indicates no apparent deviations from the established control limits, as there is no indication of an OOC condition. This result indicates that the process, in this particular case, is in the IC state at $\hat{\theta} = 1.60$. To determine how well the proposed chart can detect small changes in a real-world data application, eight new values were randomly selected from the Maxwell distribution with a fixed scale parameter of $\hat{\theta} = 1.90$. The value $\hat{\theta} = 1.90$ represents a 20% increase in the monitoring parameter for the underlying Maxwell DGP. The observations, including the IC and OOC samples, are plotted via the proposed chart and an existing chart, as shown in Fig. 11.

The proposed chart presented in Fig. 11(a) demonstrates that all data points beyond the 14th sample show an upward trend above the central line, indicating that the process is in an OOC state. On the other hand, Fig. 11(b) shows that the existing V_{SQ} chart still reflects an IC state despite a shift in the scale parameter value after the 14th sample. This again highlights the sensitivity of the proposed chart in detecting even minor changes in the parameter compared with the existing V_{SQ} chart.

9. Concluding remarks

In this study, we propose a novel design referred to as the MXEWMA chart with the intention of tracking changes in the scaling parameter of a Maxwell process. The chart depicts the sampling distribution of the maximum likelihood estimator pertaining to the Maxwell quality characteristic within the structure of the EWMA model. To facilitate the practical application of our design, we derived several formulas

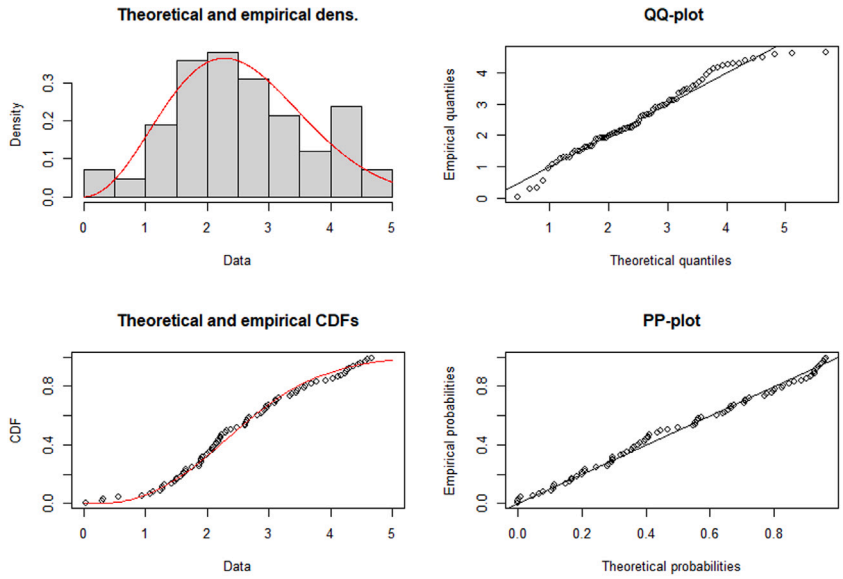

Fig. 9. Basic probability plots of the failure times of aircraft windshields.

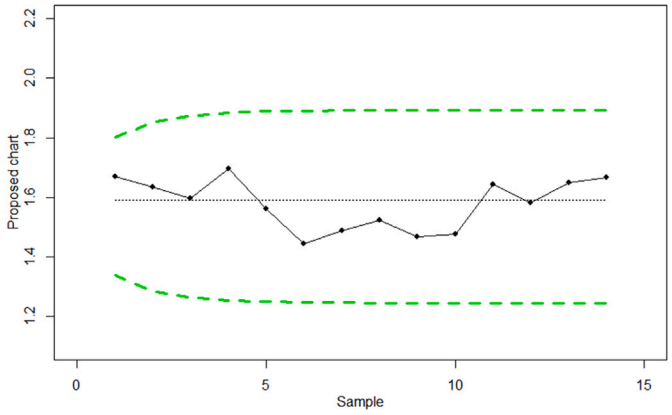

Fig. 10. Monitoring of windshield failure measurements via the proposed chart.

and established specific control limits. Our proposed chart offers a superior alternative to the existing counterpart, specifically in its ability to detect minor shifts in the studied parameter. Assuming Maxwell output data, the design parameters of the MXEWMA chart are derived for a range of sample sizes. By means of Monte Carlo simulation, we analyzed key statistical characteristics of the proposed chart, including the MRL, ARL, and SDRL, to determine how well it performs. The numerical analysis shows that the proposed chart is more effective with larger sample sizes. The MXEWMA chart outperforms the existing method for identifying minor changes in the study parameter, as shown by the simulation analysis. The proposed chart was compared with its counterpart in terms of its power profiles. This comparative assessment led to the conclusion that the MXEWMA offers a highly efficient means of detecting minor to moderate changes in the scale factor of Maxwell quality characteristics. The proposed chart was also investigated for parameter estimation. The results demonstrate that parameter estimation impacts the control chart's performance, requiring larger subgroup sizes to achieve nominal IC performance metrics, particularly in terms of ARL_0 stability. Finally, a real-world dataset on the failure process of aircraft windshields was employed to demonstrate the practical application of the proposed chart in the industrial sector. The proposed control chart outperforms the existing model in detecting small changes in process parameters, making it more effective for real-world applications.

While the proposed MXEWMA chart is effective at detecting smaller shifts in the scale parameter of Maxwell processes, it has a potential limitation known as the inertia problem. To address this, adaptive schemes that adjust the weights of past observations on the basis of the magnitude of the error could be developed (Saghir et al., 2024). These schemes enhance the chart's performance in detecting both small and large changes simultaneously. Future research could focus on incorporating these adaptive methods into the MXEWMA chart to effectively moderate the inertia issue and improve its ability to monitor shifts, whether minor or major, in Maxwell processes.

CRediT authorship contribution statement

Zahid Khan: Writing – review & editing, Writing – original draft, Software, Methodology, Investigation, Data curation, Conceptualization. **Aamir Saghir:** Writing – original draft, Methodology, Formal analysis. **Attila Katona:** Writing – original draft, Visualization, Data curation. **Zsolt T. Kosztyán:** Writing – review & editing, Writing – original draft, Supervision.

Funding

This work was created as part of the TKP2021-NVA-10 project with support provided by the Ministry of Culture and Innovation of Hungary from the National Research, Development and Innovation Fund, Hungary, financed under the 2021 Thematic Excellence Program funding scheme.

Acknowledgments

The authors would like to thank the Area Editor and the anonymous reviewers for their valuable feedback and suggestions, which significantly enhanced the quality of this paper. The authors also extend their gratitude for the support provided by the TKP2021-NVA-10 project under the 2021 Thematic Excellence Programme, as well as by project no. BME-NVA-02, funded by the National Research, Development, and Innovation Fund of Hungary. Additionally, the authors are grateful for the support of the European Union project RRF-2.3.1-21-2022-00004, carried out within the framework of the Artificial Intelligence National Laboratory.

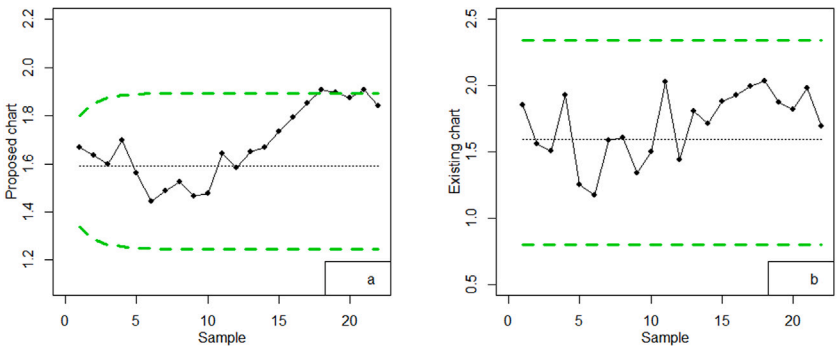

Fig. 11. Monitoring of windshield failure measurements with a 20% increase in the target parameter.

Data availability

Data supporting the findings of this study are available within the article.

References

Abbas, N. (2018). Homogeneously weighted moving average control chart with an application in substrate manufacturing process. *Computers & Industrial Engineering*, *120*, 460–470. http://dx.doi.org/10.1016/j.cie.2018.05.009.

Abbas, Z., Abbas, N., Nazir, H. Z., & Riaz, M. (2024). Parametric and nonparametric versions of adaptive CUSUM charts for monitoring the location of individual measurements. *Journal of Statistical Computation and Simulation*, 1–28. http://dx.doi.org/10.1080/00949655.2024.2347419.

Abbas, Z., Nazir, H. Z., Akhtar, N., Riaz, M., & Abid, M. (2020). On developing an exponentially weighted moving average chart under progressive setup: An efficient approach to manufacturing processes. *Quality and Reliability Engineering International*, *36*(7), 2569–2591. http://dx.doi.org/10.1002/qre.2716.

Abbas, Z., Nazir, H. Z., Riaz, M., Shi, J., & Abdisa, A. G. (2023). An unbiased function-based Poisson adaptive EWMA control chart for monitoring range of shifts. *Quality and Reliability Engineering International*, *39*(6), 2185–2201. http://dx.doi.org/10.1002/qre.3320.

Abbas, Z., Nazir, H. Z., Xiang, D., & Shi, J. (2024). Nonparametric adaptive cumulative sum charting scheme for monitoring process location. *Quality and Reliability Engineering International*, http://dx.doi.org/10.1002/qre.3522.

Abbas, N., Riaz, M., & Does, R. J. (2011). Enhancing the performance of EWMA charts. *Quality and Reliability Engineering International*, *27*(6), 821–833. http://dx.doi.org/10.1002/qre.1175.

Abbas, T., Zaman, B., Atir, A., Riaz, M., & Akbar Abbasi, S. (2019). On improved dispersion control charts under ranked set schemes for normal and non-normal processes. *Quality and Reliability Engineering International*, *35*(5), 1313–1341. http://dx.doi.org/10.1002/qre.2531.

Abbasi, S. A., & Miller, A. (2012). On proper choice of variability control chart for normal and non-normal processes. *Quality and Reliability Engineering International*, *28*(3), 279–296. http://dx.doi.org/10.1002/qre.1244.

Adeoti, O. A. (2020). On control chart for monitoring exponentially distributed quality characteristic. *Transactions of the Institute of Measurement and Control*, *42*(2), 295–305. http://dx.doi.org/10.1177/0142331219868.

Ahmed, F., Mahmood, T., Riaz, M., & Abbas, N. (2024). Comprehensive review of high-dimensional monitoring methods: trends, insights, and interconnections. *Quality Technology & Quantitative Management*, 1–25. http://dx.doi.org/10.1080/16843703.2024.2395745.

Ahmed, A., Sanaullah, A., & Hanif, M. (2020). A robust alternate to the HEWMA control chart under non-normality. *Quality Technology & Quantitative Management*, *17*(4), 423–447. http://dx.doi.org/10.1080/16843703.2019.1662218.

Facility Supplier for Aircraft Company, T. (2023). C&L aviation group. https://cla.aero/. (Accessed 16 June 2024).

Al-Kzzaz, H., & Abd El-Monsef, M. (2022). Inverse power Maxwell distribution: statistical properties, estimation and application. *Journal of Applied Statistics*, *49*(9), 2287–2306. http://dx.doi.org/10.1080/02664763.2021.1899143.

Alduais, F. S., & Khan, Z. (2023). EWMA control chart for Rayleigh process with engineering applications. *IEEE Access*, *11*, 10196–10206. http://dx.doi.org/10.1109/ACCESS.2023.3240660.

Alevizakos, V., Chatterjee, K., Koukouvinos, C., & Lappa, A. (2022). A double moving average control chart: Discussion. *Communications in Statistics. Simulation and Computation*, *51*(10), 6043–6057. http://dx.doi.org/10.1080/03610918.2020.1788591.

Alevizakos, V., Chatterjee, K., Koukouvinos, C., & Lappa, A. (2023). The effect of parameters estimation on the performance of variables control charts under repetitive sampling. *Communications in Statistics. Theory and Methods*, *52*(7), 2379–2401. http://dx.doi.org/10.1080/03610926.2021.1952269.

Arafat, S. Y., Hossain, M. P., Ajadi, J. O., & Riaz, M. (2019). On the development of EWMA control chart for Inverse Maxwell distribution. *Journal of Testing and Evaluation*, *49*, 1–18. http://dx.doi.org/10.1520/JTE20190082.

Bogo, A. B., Henning, E., & Kalbusch, A. (2023). Statistical parametric and non-parametric control charts for monitoring residential water consumption. *Scientific Reports*, *13*(1), 13543. http://dx.doi.org/10.1038/s41598-023-40584-w.

Elshahhat, A., Abo-Kasem, O. E., & Mohammed, H. S. (2023). Reliability analysis and applications of generalized Type-II progressively hybrid Maxwell–Boltzmann censored data. *Axioms*, *12*(7), 618. http://dx.doi.org/10.3390/axioms12070618.

Gan, F. (1990). Monitoring observations generated from a binomial distribution using modified exponentially weighted moving average control chart. *Journal of Statistical Computation and Simulation*, *37*(1–2), 45–60. http://dx.doi.org/10.1080/00949659008811293.

Godase, D. G., Mahadik, S. B., & Rakitzis, A. C. (2022). The SPRT control charts for the Maxwell distribution. *Quality and Reliability Engineering International*, *38*(4), 1713–1728. http://dx.doi.org/10.1002/qre.3047.

Haq, A., Abidin, Z. U., & Khoo, M. B. (2019). An enhanced EWMA-t control chart for monitoring the process mean. *Communications in Statistics. Theory and Methods*, *48*(6), 1333–1350. http://dx.doi.org/10.1080/03610926.2018.1429631.

Horng Shiau, J.-J., & Ya-Chen, H. (2005). Robustness of the EWMA control chart to non-normality for autocorrelated processes. *Quality Technology & Quantitative Management*, *2*(2), 125–146. http://dx.doi.org/10.1080/16843703.2005.11673089.

Hossain, M. P., Omar, M. H., & Riaz, M. (2017). New V control chart for the Maxwell distribution. *Journal of Statistical Computation and Simulation*, *87*(3), 594–606. http://dx.doi.org/10.1080/00949655.2016.1222391.

Hossain, M. P., & Riaz, M. (2021). On designing a new VEWMA control chart for efficient process monitoring. *Computers & Industrial Engineering*, *162*, Article 107751. http://dx.doi.org/10.1016/j.cie.2021.107751.

Hossain, M. P., Sanusi, R. A., Omar, M. H., & Riaz, M. (2019). On designing Maxwell CUSUM control chart: an efficient way to monitor failure rates in boring processes. *International Journal of Advanced Manufacturing Technology*, *100*, 1923–1930. http://dx.doi.org/10.1007/s00170-018-2679-1.

Human, S. W., Kritzinger, P., & Chakraborti, S. (2011). Robustness of the EWMA control chart for individual observations. *Journal of Applied Statistics*, *38*(10), 2071–2087. http://dx.doi.org/10.1080/02664763.2010.545114.

Javed, A., Abbas, T., & Abbas, N. (2024). Developing Bayesian EWMA chart for change detection in the shape parameter of Inverse Gaussian process. *PLoS One*, *19*(5), Article e0301259. http://dx.doi.org/10.1371/journal.pone.0301259.

Jensen, W. A., Jones-Farmer, L. A., Champ, C. W., & Woodall, W. H. (2006). Effects of parameter estimation on control chart properties: a literature review. *Journal of Quality Technology*, *38*(4), 349–364. http://dx.doi.org/10.1080/00224065.2006.11918623.

Jones-Farmer, L. A., Woodall, W. H., Steiner, S. H., & Champ, C. W. (2014). An overview of phase I analysis for process improvement and monitoring. *Journal of Quality Technology*, *46*(3), 265–280. http://dx.doi.org/10.1080/00224065.2014.11917969.

Kapase, R. A., & Ghute, V. B. (2024). Identifying the time of step change in process parameter for Maxwell distribution. *Journal of Statistical Computation and Simulation*, *94*(7), 1631–1644. http://dx.doi.org/10.1080/00949655.2023.2294949.

Katona, A. I., Saghir, A., Hegedűs, C., & Kosztyán, Z. T. (2023). Design of risk-based univariate control charts with measurement uncertainty. *IEEE Access*, http://dx.doi.org/10.1109/ACCESS.2023.3312226.

Knoth, S. (2021). Steady-state average run length (s): Methodology, formulas, and numerics. *Sequential Analysis*, *40*(3), 405–426. http://dx.doi.org/10.1080/07474946.2021.1940501.

Kosztyán, Z. T., & Katona, A. I. (2018). Risk-based X-bar chart with variable sample size and sampling interval. *Computers & Industrial Engineering*, *120*, 308–319. http://dx.doi.org/10.1016/j.cie.2018.04.052.

Liu, J. Y., Xie, M., Goh, T. N., & Chan, L. (2007). A study of EWMA chart with transformed exponential data. *International Journal of Production Research*, *45*(3), 743–763. http://dx.doi.org/10.1080/00207540600792598.

Lu, X., Zhang, Y., & Zhang, Z. (2024). Effect on damage of aircraft windshield impacted by light UAV with different postures. *Aeronautical Journal*, *128*(1322), 771–787. http://dx.doi.org/10.1017/aer.2023.65.

Mahmood, T., & Erem, A. (2023). A bivariate exponentially weighted moving average control chart based on exceedance statistics. *Computers & Industrial Engineering*, *175*, Article 108910. http://dx.doi.org/10.1016/j.eswa.2023.119660.

Maravelakis, P. E., Panaretos, J., & Psarakis, S. (2005). An examination of the robustness to non normality of the EWMA control charts for the dispersion. *Communications in Statistics—Simulation and Computation®*, *34*(4), 1069–1079. http://dx.doi.org/10.1080/03610910500308719.

Mehmood, R., Mpungu, K., Ali, I., Zaman, B., Qureshi, F. H., & Khan, N. (2023). A new approach for designing the Shewhart-type control charts with generalized sensitizing rules. *Computers & Industrial Engineering*, *182*, Article 109379. http://dx.doi.org/10.1016/j.cie.2023.109379.

Montgomery, D. C. (2019). *Introduction to statistical quality control* (8th ed.). Wiley.

Murthy, D. P., Xie, M., & Jiang, R. (2004). *Weibull models*. John Wiley & Sons, http://dx.doi.org/10.1002/047147326X.

Nawaz, M. S., Azam, M., & Aslam, M. (2021). EWMA and DEWMA repetitive control charts under non-normal processes. *Journal of Applied Statistics*, *48*(1), 4–40. http://dx.doi.org/10.1080/02664763.2019.1709809.

Nazir, H. Z., Abid, M., Akhtar, N., Riaz, M., & Qamar, S. (2021). An efficient mixed-memory-type control chart for normal and non-normal processes. *Scientia Iranica*, *28*(3), 1736–1749. http://dx.doi.org/10.24200/sci.2019.51437.2177.

Noiplab, T., & Mayureesawan, T. (2019). Modified EWMA control chart for skewed distributions and contaminated processes. *Thailand Statistician*, *17*(1), 16–29.

Raza, S. M. M., Riaz, M., & Ali, S. (2016). EWMA control chart for Poisson–exponential lifetime distribution under type I censoring. *Quality and Reliability Engineering International*, *32*(3), 995–1005. http://dx.doi.org/10.1002/qre.1809.

Riaz, M., & Does, R. J. (2009). A process variability control chart. *Computational Statistics*, *24*, 345–368. http://dx.doi.org/10.1007/s00180-008-0122-z.

Ruhi, S., Sarker, S., & Karim, M. (2015). Mixture models for analyzing product reliability data: a case study. *SpringerPlus*, *4*, 1–14. http://dx.doi.org/10.1186/s40064-015-1420-x.

Ryan, A. G., & Woodall, W. H. (2010). Control charts for Poisson count data with varying sample sizes. *Journal of Quality Technology*, *42*(3), 260–275. http://dx.doi.org/10.1080/00224065.2010.11917823.

Saghir, A., Ahmad, L., & Aslam, M. (2021). Modified EWMA control chart for transformed gamma data. *Communications in Statistics. Simulation and Computation*, *50*(10), 3046–3059. http://dx.doi.org/10.1080/03610918.2019.1619762.

Saghir, A., Akber Abbasi, S., & Faraz, A. (2021). The exact method for designing the Maxwell chart with estimated parameter. *Communications in Statistics. Simulation and Computation*, *50*(1), 270–281. http://dx.doi.org/10.1080/03610918.2018.1554114.

Saghir, A., Hu, X., Tran, K. P., & Song, Z. (2023). Optimal design and evaluation of adaptive EWMA monitoring schemes for inverse Maxwell distribution. *Computers & Industrial Engineering*, *181*, Article 109290. http://dx.doi.org/10.1016/j.cie.2023.109290.

Saghir, A., Khan, Z., Hu, X., & Johannssen, A. (2024). Adaptive EWMA control charts for the Rayleigh distribution. *Computers & Industrial Engineering*, Article 110505. http://dx.doi.org/10.1016/j.cie.2024.110505.

Sanaullah, A., Chaudhary, A. M., Hanif, M., & Sharma, P. (2024). EWMA control charts based on robust estimators: A powerful tool for monitoring a process with a non-normal distribution. *Journal of Computational and Applied Mathematics*, *449*, Article 115919. http://dx.doi.org/10.1016/j.cam.2024.115919.

Shah, F., Khan, Z., Aslam, M., & Kadry, S. (2021). Development of the -control chart for extreme data with an application to the carbon fiber industry. *Mathematical Problems in Engineering*, *2021*, 594–606. http://dx.doi.org/10.1155/2021/9766986.

Sharma, V. K., Dey, S., Singh, S. K., & Manzoor, U. (2018). On length and area-biased maxwell distributions. *Communications in Statistics. Simulation and Computation*, *47*(5), 1506–1528. http://dx.doi.org/10.1080/03610918.2017.1317804.

Teoh, J. W., Teoh, W. L., Khoo, M. B., Celano, G., & Chong, Z. L. (2023). Optimal designs of the omnibus SPRT control chart for joint monitoring of process mean and dispersion. *International Journal of Production Research*, 1–24. http://dx.doi.org/10.1080/00207543.2023.2254855.

Tomer, S. K., & Panwar, M. (2020). A review on Inverse Maxwell distribution with its statistical properties and applications. *Journal of Statistical Theory and Practice*, *14*, 1–25. http://dx.doi.org/10.1007/s42519-020-00100-z.